

Estimation of Mobile Speed and Average Received Power in Wireless Systems Using Best Basis Methods*

Ravi Narasimhan and Donald C. Cox
Department of Electrical Engineering
Stanford University, Stanford, CA 94305-9515 USA
nkravi@wireless.stanford.edu, dcox@spark.stanford.edu

Abstract

A new method is presented for estimating the mobile speed and the average received power in general wireless environments. The locally stationary received signal is expanded into a local exponential basis using best basis methods. An estimate of the time-varying Doppler spectrum is obtained together with an estimate of the maximum Doppler frequency, which is proportional to the mobile speed. The average received power is then estimated by integrating the time-varying spectrum. Simulations demonstrate good tracking of variable mobile speed and average received power for a wide range of angular distributions of incident power. The speed and power estimates are also used to detect the corner effect in urban cellular systems to improve handoff performance and reduce the call dropping rate.

1. Introduction

Estimates of the mobile speed and the average received power are useful to increase the realized wireless communication system capacity by improving the performance of handoff, power control and channel assignment algorithms. In many environments, the received signal consists of a sum of waves which have been reflected by objects such as mountains, trees and buildings. The sum of many waves at the receiver gives rise to small-scale spatial variation of the received envelope (on the order of a wavelength). The received signal is nonstationary for distances on the order of building sizes since the mean of the small-scale variation changes considerably. This large-scale variation of the mean is known as shadowing. The mean of the shadowing also decreases as the distance between the base station and the mobile station increases.

Previous approaches to mobile speed estimation assume

*This work was supported by a National Science Foundation Graduate Research Fellowship.

specific angular distributions of incident power [1, 5]. The average received power is the local mean of the small-scale variation (up to a constant) and represents the distance-dependent trend and the shadowing. An adaptive method to estimate the average power is proposed in [5]. This method assumes Rayleigh fading with a uniform angular distribution of incident power in a plane. The literature mentioned above has considered only the problem of a constant, unknown mobile speed. Recently, methods have been introduced to track variable mobile speed and average received power without requiring adaptive estimation windows [9, 8]. While overcoming the restrictions of a constant mobile speed, these techniques, like all the others in the literature, assume Rayleigh fading with a uniform angular distribution of incident power in a plane.

A new method of estimating and tracking the mobile speed and the average received power is described in this paper. This method uses the local stationarity of the received signal and does not assume a specific angular distribution of incident power. The signal is expanded into a basis of smooth local complex exponentials using best basis methods [7, 4] to obtain an estimate of the time-varying Doppler spectrum. The time-varying spectrum yields estimates of the mobile speed and the average received power as a function of time. These estimates are then applied to the detection of the corner effect in urban cellular systems. The corner effect refers to a sudden change in the average received power when a mobile station makes a turn at an intersection. Timely detection of the corner effect can initiate a handoff to a nearby base station to reduce the call dropping rate.

The paper is organized as follows. In Section 2, wireless propagation and noise models are presented. Section 3 presents a method to estimate the time-varying spectrum, the mobile speed and the average received power. Section 4 determines relevant parameters and presents performance results for variable mobile speed. A corner detection method is described in Section 5. Section 6 concludes the paper.

2. Wireless propagation and noise models

The macrocellular model discussed here takes into account three effects which are present in many macrocellular wireless environments: correlated multipath fading, correlated log-normal shadowing, and a distance-dependent trend [6]. The received bandpass signal at a mobile station consists of a sum of contributions from several paths. Let $s(\theta)$ denote the distribution of incident power in angle θ in a plane. For a transmitting base station located at \mathbf{x}_B , let $p(\mathbf{x}, \mathbf{x}_B)$ be the received power at the mobile station averaged over a small neighborhood of \mathbf{x} . Let λ represent the carrier wavelength and $r_c(\mathbf{x})$ denote the noiseless received complex envelope. A model for $r_c(\mathbf{x})$ is constructed using a weighted sum of plane waves arriving at different angles θ . The weight for each angle θ is proportional to $\sqrt{p(\mathbf{x}, \mathbf{x}_B)s(\theta)}$. The time waveform is generated using $r_c(\mathbf{x})$ with the position $\mathbf{x} = \mathbf{x}(t)$ varying according to the mobile velocity.

The average received power $p(\mathbf{x}, \mathbf{x}_B)$ contains the distance-dependent trend and the log-normal shadowing. Let γ represent the exponent of the distance-dependent trend. Furthermore, let $10^{L(\mathbf{x}, \mathbf{x}_B)/10}$ denote the log-normal shadowing between the locations \mathbf{x} and \mathbf{x}_B . The received power averaged over a neighborhood of \mathbf{x} due to the base station located at \mathbf{x}_B can then be expressed as

$$p(\mathbf{x}, \mathbf{x}_B) = P_0 \|\mathbf{x} - \mathbf{x}_B\|^{-\gamma} 10^{L(\mathbf{x}, \mathbf{x}_B)/10} \quad (1)$$

where P_0 accounts for antenna parameters, transmitted power, and other relevant system parameters. The process $L(\mathbf{x}, \mathbf{x}_B)$ is modelled as an exponentially correlated, zero-mean Gaussian random process which is wide-sense stationary in the variable \mathbf{x} .

The microcellular model described in [2] is used to evaluate the corner detection method of Section 5. As in the macrocellular case, the average power $p(\mathbf{x}, \mathbf{x}_B)$ consists of a distance-dependent trend and log-normal shadowing before and after the mobile station makes a turn at an intersection. At the intersection, the corner effect results in a signal drop of ΔS dB in y_0 meters.

The noise model developed here is based on a receiver model for a digital wireless system in which the received complex envelope is processed as follows. Baseband Gaussian noise $n_{BB}(t)$ is added to the noiseless complex envelope. The bandwidth of $n_{BB}(t)$ is $1/T$, where T is the symbol duration of the digitally modulated waveform. To reduce the effect of noise in the speed estimates, the signal is passed through a unit-gain, square-root raised cosine lowpass Doppler filter with bandwidth $f_D(1 + \alpha)/(1 - \alpha)$. The maximum Doppler frequency at the highest speed of interest is f_D , and the excess bandwidth factor is α with $0 < \alpha < 1$. The Doppler filter frequency response is flat

over the bandwidth of the complex envelope. We also define $T_D = (1 - \alpha)/(2f_D)$. The output of the filter is $r(t)$. Each quadrature component of the noise at the filter output has variance σ_n^2 .

3. Estimation of time-varying spectrum, mobile speed and average received power

The signal $r(t)$ is locally stationary since the average received power $p(\mathbf{x}, \mathbf{x}_B)$ varies slowly. It is shown in [7] that there exists a basis of local cosine (or sine) functions that "almost diagonalizes" the covariance matrix of a locally stationary process. This fact is used in [4] to estimate the covariance of a locally stationary process from sampled data. Here, we estimate the time-varying spectrum of $r(t)$ using a modified version of the covariance estimation technique described in [4]. The time-varying spectrum is then used to estimate and track the mobile speed and the average received power as described below.

The signal $r(t)$ is sampled at rate $1/T_s$ to form $r[n]$. We consider blocks of $r[n], n \in \{0, 1, \dots, N-1\}$, where N is a dyadic length: $N = 2^M$. A recursive dyadic partition of the interval $I_{0,0} = \{0, 1, \dots, N-1\}$ is obtained as follows [3]. For each m satisfying $0 \leq m \leq M$, dyadic subintervals of $I_{0,0}$ with length $N2^{-m}$ are given by

$$I_{m,l} = \{N2^{-m}l, N2^{-m}l+1, \dots, N2^{-m}(l+1)-1\}, \quad 0 \leq l < 2^m. \quad (2)$$

The choice of M is discussed below. A recursive dyadic partition of $I_{0,0}$ is represented by $I_{0,0} = \bigcup_{m,l} I_{m,l}$, where the $I_{m,l}$ are disjoint.

Associated with each subinterval $I_{m,l}$ are two smooth window functions $b_+^{m,l}[n]$ and $b_-^{m,l}[n]$. The window functions are nonzero over the interval $I_{m,l}$ extended by $\varepsilon \in \mathbb{Z}^+$ samples beyond each endpoint of $I_{m,l}$. Smooth local exponential functions corresponding to $I_{m,l}$ are defined by

$$\begin{aligned} \psi^{m,l,k}[n] = & b_+^{m,l}[n] \sqrt{\frac{1}{N2^{-m}}} \exp \left\{ j \frac{2\pi k(n+1/2-N2^{-m}l)}{N2^{-m}} \right\} + \\ & b_-^{m,l}[n] \sqrt{\frac{1}{N2^{-m}}} \exp \left\{ -j \frac{2\pi k(n+1/2-N2^{-m}l)}{N2^{-m}} \right\}, \\ & -N2^{-m-1} \leq k < N2^{-m-1}. \end{aligned} \quad (3)$$

Let a recursive dyadic partition \mathcal{P} be denoted by $\mathcal{P} = \{I_{m,l} : (m,l) \in \zeta\}$. The window functions $b_+^{m,l}[n]$ and $b_-^{m,l}[n]$ are chosen such that if $M = \log_2 \left(\frac{N}{2\varepsilon} \right)$, then $B^\zeta = \{\psi^{m,l,k}[n]\}_{(m,l) \in \zeta, -N2^{-m-1} \leq k < N2^{-m-1}}$ forms an orthonormal basis for discrete signals having compact support in $[\varepsilon, N - \varepsilon]$. The ratio $\|b_-^{m,l}\|^2 / (\|b_+^{m,l}\|^2 + \|b_-^{m,l}\|^2)$ is kept small such that most of the energy of $\psi^{m,l,k}[n]$ is contained in the first term of (3). The second term of (3) is needed to overcome the Balian-Low obstruction for orthonormal

bases of windowed exponentials [10]. The library of bases B^ζ which correspond to different recursive dyadic partitions of $I_{0,0}$ is denoted by \mathcal{L} .

We now consider $i_{\max} \geq 1$ realizations of the received signal $\{r_i[n]\}_{i \in \{1, \dots, i_{\max}\}, n \in \{0, \dots, N-1\}}$. A fast algorithm [10] based on the fast Fourier transform (FFT) is used to calculate the inner products $\langle r_i, \psi^{m,l,k} \rangle = \sum_n r_i[n] \overline{\psi^{m,l,k}[n]}$, where the bar denotes complex conjugation. A table of empirical variances $s_{m,l,k}^2$ is then calculated by

$$s_{m,l,k}^2 = \frac{1}{i_{\max}} \sum_{i=1}^{i_{\max}} |\langle r_i, \psi^{m,l,k} \rangle|^2. \quad (4)$$

We wish to find a basis $B^{\hat{\zeta}} \in \mathcal{L}$ that ‘‘almost diagonalizes’’ the covariance matrix of $\{r_i[n]\}$. The basis $B^{\hat{\zeta}}$ is chosen to maximize a convex functional of the empirical variances:

$$B^{\hat{\zeta}} = \arg \max_{B^\zeta \in \mathcal{L}} \sum_{(m,l) \in \zeta} \sum_{k=-N2^{-m-1}}^{N2^{-m-1}-1} (s_{m,l,k}^2)^2. \quad (5)$$

The number of bases $B^\zeta \in \mathcal{L}$ is greater than $2^{M/2}$. However, there exists a fast dynamic programming algorithm [3] which selects the best orthonormal basis $B^{\hat{\zeta}}$ in $O(N \log_2 N)$ operations. The best basis corresponds to a particular partitioning $\hat{\mathcal{P}}$ of the interval $I_{0,0}$. We obtain a coarse estimate of the time-varying spectrum by associating $s_{m,l,k}^2$ with each time-frequency tile $[NT_s 2^{-m} l, NT_s 2^{-m} (l+1)) \times [(k-1/2)/(NT_s 2^{-m}), (k+1/2)/(NT_s 2^{-m})]$ in the basis $B^{\hat{\zeta}}$. The basis element $\psi^{m,l,k}$ has most of its energy concentrated in this tile.

An estimate of the maximum Doppler frequency and, hence, the mobile speed are obtained using the time-varying spectrum as follows. For a mobile speed v and a wavelength λ , the maximum Doppler frequency f_{\max} is $f_{\max} = v/\lambda$. In some propagation environments, there is no significant power at incident angles of 0 or π with respect to the mobile velocity. In such cases, the bandwidth of the time-varying spectrum is less than the maximum Doppler frequency. For robust estimation of the mobile speed and the average received power in these situations, the received complex envelopes from two antennas are used. The signals from the two antennas yield $i_{\max} = 2$ realizations: $r_1[n]$ and $r_2[n]$.

We consider the estimate of the time-varying spectrum for a subinterval $I_{m,l} \in \hat{\mathcal{P}}$. The estimates of the maximum Doppler frequency and the average received power are placed at the midpoint in time of the time-frequency tiles associated with $I_{m,l}$, i.e., at time $t_0 = NT_s 2^{-m} (l+1/2)$. The duration of the smallest subinterval is determined by the maximum acceptable uncertainty in frequency Δf_{\max} . We let $\{c_i\}_{i=1, \dots, i_{\max}}$ denote the local maxima of $\{s_{m,l,k}^2\}$ (for fixed m and l) with the c_i 's sorted in decreasing order. The center frequency of the time-frequency tile associated with

c_i is $f_i = k_i/(NT_s 2^{-m})$. The Doppler frequency f_i of an incoming wave is related to its angle of arrival θ_i (with respect to the mobile velocity) by $f_i = f_{\max} \cos \theta_i$. The two-element antenna array (oriented along the mobile velocity) is used to estimate the angles θ_i for the local maxima c_i . The separation distance between the antenna elements is $\delta < \lambda/2$. The phase difference $\Delta \Phi_i$ for frequency f_i between the signals received at the two antennas is estimated by

$$\Delta \Phi_i = \arg \left(\langle r_2, \psi^{m,l,k_i} \rangle \right) - \arg \left(\langle r_1, \psi^{m,l,k_i} \rangle \right). \quad (6)$$

An estimate for $\cos \theta_i$ is then $\widehat{\cos \theta}_i = \Delta \Phi_i / (2\pi \delta / \lambda)$.

In order to separate the local maxima c_i due to noise from the local maxima due to the angular distribution of incident power, the following method is adopted. If $c_2/c_1 < \tau_1$, only the largest local maximum c_1 is declared to be due to the distribution of incident power. This situation would arise, for instance, when there is a line of sight between the base and mobile stations. The selection of the threshold τ_1 is discussed in Section 4. The estimate of the maximum Doppler frequency at time t_0 for this case is

$$\widehat{f}_{\max}(t_0) = \begin{cases} |f_1 / \widehat{\cos \theta}_1|, & 0 < |\widehat{\cos \theta}_1| \leq 1 \\ |f_1|, & \text{otherwise.} \end{cases} \quad (7)$$

If $c_2/c_1 \geq \tau_1$, we identify all local maxima $\{c_i\}_{i=1,2, \dots, i_{\tau_2}}$ satisfying another threshold condition, i.e., $c_i/c_2 \geq \tau_2$ for $i = 1, 2, \dots, i_{\tau_2}$ and $0 \leq \tau_2 \leq 1$. This condition is imposed to provide robustness to noise while being able to handle a dominant multipath component. The choice of τ_2 is also discussed in Section 4. An estimate of the maximum Doppler frequency for this case is given by

$$\widehat{f}_{\max}(t_0) = \max \left\{ |f_1|, \text{med}_{i=1,2, \dots, i_{\tau_2}, 0 < |\widehat{\cos \theta}_i| \leq 1} \left| \frac{f_i}{\widehat{\cos \theta}_i} \right| \right\} \quad (8)$$

where ‘‘med’’ stands for median. Now, suppose that $\widehat{f}_{\max}(t_0) \geq |k/(NT_s 2^{-m})|$, $0 \leq |k| \leq k_{\max}$. The estimate of the average received power at time t_0 is given by

$$\hat{p}(t_0) = \frac{1}{N2^{-m+1}} \sum_{k=-k_{\max}}^{k_{\max}} s_{m,l,k}^2. \quad (9)$$

Estimates of the maximum Doppler frequency and the average received power are obtained in this manner for each of the subintervals $I_{m,l} \in \hat{\mathcal{P}}$. Thus, the mobile speed estimates are $\hat{v}(t_0) = \widehat{f}_{\max}(t_0) \lambda$. To limit estimation error, speed estimates which do not satisfy a maximum acceleration constraint are discarded together with the corresponding average power estimates. The following section describes the selection of the thresholds τ_1 and τ_2 together with simulations which apply the speed and average power estimation technique.

4. Parameter selection and simulation results

The threshold τ_1 is determined by considering a wide-sense stationary, line-of-sight propagation environment. In this case, the discrete-time noiseless complex envelope is a complex exponential with average power P_r . The local maximum of the signal power spectrum is $2NP_r$, where N is the size of the signal block. From the noise model of Section 2, it can be shown that the local maximum of the noise power spectrum is $2\sigma_n^2 T_D/T_s$. Therefore, to discard the local maxima due to noise with a safety factor of F , we have $\tau_1 > FT_D/(NT_s \cdot SNR_p)$, where $SNR_p = P_r/\sigma_n^2$ is the processing signal-to-noise ratio (SNR). The SNR at the input of the Doppler filter must be at least 3–5 dB for synchronization and at least 8–10 dB for system operation. Since the lowpass filter introduces a gain of at least 20 dB in SNR, the processing SNR satisfies $SNR_p \geq 20$ dB. Using $F = 3$, $T_D/T_s = 5$, $N = 512$ and $SNR_p = 20$ dB, we have $\tau_1 > 3 \times 10^{-4}$. A value of $\tau_1 = 10^{-3}$ is chosen.

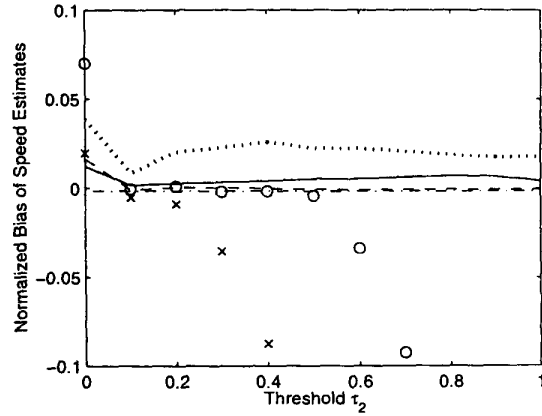
The second threshold τ_2 is selected by simulations using the following six angular distributions of incident power:

$$\begin{aligned} s_a(\theta) &= 1/(2\pi)\text{rect}(\theta/(2\pi)) \\ s_b(\theta) &= (10/11)\delta(\theta - \pi/3) + 1/(22\pi)\text{rect}(\theta/(2\pi)) \\ s_c(\theta) &= \delta(\theta - 3\pi/4) \\ s_d(\theta) &= 1.5\cos(3\theta)\text{rect}(3\theta/\pi) \\ s_e(\theta) &= (10/11)\delta(\theta - \pi/2) + 1/(22\pi)\text{rect}(\theta/(2\pi)) \\ s_f(\theta) &= 1.5\cos(3(\theta - \pi/2))\text{rect}(3(\theta - \pi/2)/\pi) \end{aligned} \quad (10)$$

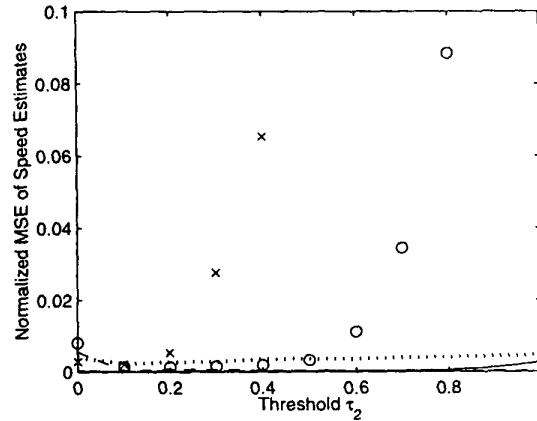
where $\delta(\cdot)$ denotes the Dirac delta function. Rayleigh fading with a uniform two-dimensional (2-D) angular distribution is represented by $s_a(\theta)$. Distributions $s_b(\theta)$ and $s_e(\theta)$ represent Rician fading with Rice factor 10 and dominant component at angles of $\pi/3$ and $\pi/2$, respectively, with respect to the mobile velocity. A line-of-sight component with an angle of $3\pi/4$ is described by $s_c(\theta)$. Finally, $s_d(\theta)$ and $s_f(\theta)$ represent Rayleigh fading with nonuniform 2-D angular distributions centered at 0 and $\pi/2$, respectively.

In order to select the threshold τ_2 independently of the mobile speed, spatial sampling at a constant interval is used. In addition, the average received signal power and noise power are kept constant such that $SNR_p = 20$ dB. For each angular distribution of incident power, 20 realizations are simulated, each having 50 speed and average power estimates (a total of 1000 speed and average power estimates per distribution). The separation distance between estimates is 51.2λ .

The normalized bias and mean square error (MSE) of the speed estimates are $E[\hat{v}/v - 1]$ and $E[(\hat{v}/v - 1)^2]$, respectively. For the angular distributions considered, Fig. 1 plots the normalized bias and MSE of the speed estimates as τ_2 is varied. The negative biases observed for $s_e(\theta)$ and



(a)



(b)

Figure 1. (a) Normalized bias and (b) normalized mean square error of speed estimates as a function of threshold τ_2 . Solid: $s_a(\theta)$; dotted: $s_b(\theta)$; dash-dot: $s_c(\theta)$; dashed: $s_d(\theta)$; 'x': $s_e(\theta)$; 'o': $s_f(\theta)$.

$s_f(\theta)$ increase in magnitude with τ_2 since fewer local maxima of the spectrum are used to estimate the mobile speed, and most of the large local maxima for these distributions are concentrated near a Doppler frequency of 0 Hz. For the line-of-sight distribution $s_c(\theta)$, the bias and MSE do not vary as a function of τ_2 since the local maxima due to noise are discarded using the first threshold ($c_2/c_1 < \tau_1$); thus, the second threshold τ_2 is never used for this distribution.

The bias and MSE of the average power estimates are

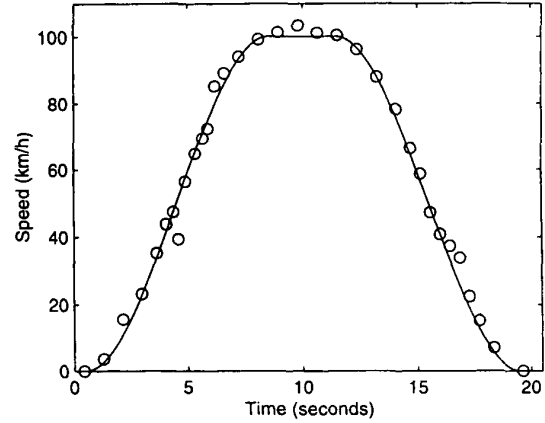
also studied as a function of τ_2 . Relatively large magnitude bias and MSE are observed in the average power estimates for the distribution $s_d(\theta)$. The reason is that for this distribution, the mean distance between the local minima of the *squared envelope* $|r_c(\mathbf{x})|^2$ is around 13λ . The mean distance between the local minima of $|r_c(\mathbf{x})|^2$ for the other distributions (except for the line-of-sight case) is on the order of $\lambda/2-2\lambda$. Thus, the averaging distance of 51.2λ does not completely remove the small-scale amplitude variations present for the distribution $s_d(\theta)$, and the result is a large magnitude bias and MSE for the estimates of the average received power. In contrast, the correlation length of the *complex envelope* $r_c(\mathbf{x})$ for the distribution $s_d(\theta)$ is on the order of $\lambda/2$. Therefore, there is neither a large bias nor a large MSE for the speed estimates since a distance of 51.2λ contains several correlation lengths of the complex envelope, which is used to estimate the mobile speed. Fig. 1 indicates a desired value of $\tau_2 = 0.1$. The normalized bias and MSE of the speed and power estimates are also investigated as SNR_p varies from 20 dB to 30 dB. No significant change in performance is observed for this range of SNR_p .

The choice of the block length N represents a trade-off between the delay in obtaining speed and power estimates and the minimum detectable non-zero speed v_{\min} . For a block length of N and a sampling period of T_s , the time-frequency tiles associated with the root interval $I_{0,0}$ have a height of $1/(NT_s)$. Therefore, the minimum detectable non-zero speed is $v_{\min} = \lambda/(2NT_s)$. Numerical values of N for speed tracking and corner detection are given below.

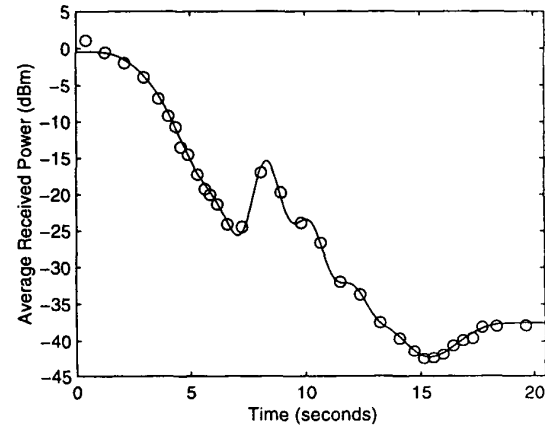
In order to demonstrate the tracking of changes in mobile speed, the speed and average power estimators are applied to a variable speed profile. Fig. 2(a) plots the true speed $v(t)$ and the speed estimates for the angular distribution $s_b(\theta)$. Fig. 2(b) plots the corresponding true average received power (in dBm) and the power estimates. Estimates which imply an acceleration of absolute value greater than $2g$ are discarded ($g \approx 9.8$ m/s is the acceleration due to gravity). The duration of each signal block used in this example is 1.706 seconds with $N = 4096$ samples ($v_{\min} = 0.35$ km/h). The maximum uncertainty in frequency is $\Delta f_{\max} = 5$ Hz, the carrier wavelength is $\lambda = 1/3$ m, the correlation length of the log-normal shadowing is 50 m, and the exponent of distance dependence is $\gamma = 4$. The results show that the estimates are able to track the variations in speed and average power well.

5. Corner detection method

This section describes a method to detect the corner effect in urban cellular systems for the propagation model of Section 2. The corner detection method uses the speed and average power estimates obtained in Section 3, except that there is no maximum acceleration constraint on the speed



(a)



(b)

Figure 2. Tracking performance of (a) mobile speed and (b) average power estimators for angular distribution $s_b(\theta)$. Solid: true mobile speed and average received power; 'o': speed and power estimates.

estimates in order to reduce the detection delay. The current and past speed estimate samples are linearly interpolated to the rate $1/T_s$. A similar interpolation is performed for the average power estimates expressed in dBm. An estimate of the distance traveled by the mobile station is obtained from the integral of the interpolated speed estimates. Using the interpolated speed and power estimates, the corner effect is detected if the average power changes by at least H_c dB in

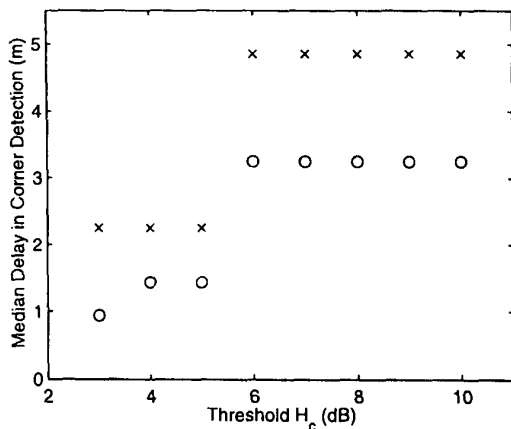


Figure 3. Median delay in detection of corner effect versus threshold H_c for two variable speed profiles. 'x': slowing down; 'o': stopping.

the last y_c meters. If the intersections in a city are separated by ΔY meters, the mobile station must travel at least ΔY meters before another corner is detected.

The corner detection algorithm is evaluated for six different microcellular propagation environments: two values ($\Delta S = 15, 20$ dB) of the signal drop at the corner are used for each of three values ($y_0 = 1.5, 3.0, 4.0$ m) of the distance over which the drop occurs. The minimum distance between intersections is $\Delta Y = 50$ m. The standard deviations for the log-normal shadowing before and after the mobile station makes a turn at the intersection are 4 dB and 7 dB, respectively.

The corner detection method is evaluated using two realistic speed profiles which capture the effects of slowing down and stopping when making a turn. For each set of propagation parameters, ten realizations of the received signal are simulated (a total of 60 realizations for each speed profile). The delay in detection is defined to be the distance from the position of the start of the signal drop to the position of the mobile station when the corner is detected. This definition includes the delay due to the block processing of the received signal (Section 4). The duration of each signal block used in the simulations is 0.427 seconds with $N = 1024$ samples. The corresponding minimum detectable non-zero speed is $v_{\min} = 1.4$ km/h.

Fig. 3 plots the median delay in corner detection versus the threshold H_c for $y_c = 3$ m. The results indicate a significant increase in the median delay as H_c is varied from 5 dB to 6 dB. Furthermore, for $H_c \geq 6$ dB, some corners are not detected. For $H_c \leq 4$ dB, there is a significant number of false corner detections since, at very low thresholds H_c ,

the shadowing is mistaken for a corner. Therefore, for the microcellular propagation environments considered here, a desired value for the threshold is $H_c = 5$ dB. The corresponding median delays are 2.25 m and 1.44 m for mobile stations slowing down and stopping, respectively.

6. Conclusions

A new technique is described for estimating the mobile speed and the average received power in general wireless environments. The method uses the local stationarity of the received signal to obtain an expansion into a basis of smooth local exponential functions. The coefficients of the expansion provide an estimate of the time-varying Doppler power spectrum. The time-varying spectrum and a two-element antenna array are used to estimate and track the mobile speed and the average received power.

The above technique is used to detect the corner effect present in urban cellular systems. A corner is detected if the average received power changes by a significant amount within a short distance. Simulations demonstrate that this method detects corners with small delay and, hence, is useful in reducing handoff delay and the call dropping rate.

References

- [1] M. D. Austin and G. L. Stuber. Velocity adaptive handoff algorithms for microcellular systems. *IEEE Trans. Veh. Technol.*, 43(3):549–561, 1994.
- [2] J.-E. Berg, R. Bownds, and F. Lotse. Path loss and fading models for microcells at 900 mhz. In *IEEE Veh. Technol. Conf.*, pages 666–671, May 1992.
- [3] R. Coifman and M. V. Wickerhauser. Entropy based algorithms for best basis selection. *IEEE Trans. Infor. Theory*, 38(2):713–718, 1992.
- [4] D. L. Donoho, S. Mallat, and R. von Sachs. Estimating covariances of locally stationary processes: consistency of best basis methods. Manuscript, Feb. 1998.
- [5] J. M. Holtzman and A. Sampath. Adaptive averaging methodology for handoffs in cellular systems. *IEEE Trans. Veh. Technol.*, 44(1):59–66, 1995.
- [6] W. C. Jakes. *Microwave Mobile Communications*. Wiley, New York, NY, 1974.
- [7] S. Mallat, G. Papanicolaou, and Z. Zhang. Adaptive covariance estimation of locally stationary processes. *Ann. Statis.*, 26(1):1–47, 1998.
- [8] R. Narasimhan and D. C. Cox. Estimation of the nonstationary mean signal in wireless systems using wavelets. In *IEEE Global Commun. Conf.*, Dec. 1999.
- [9] R. Narasimhan and D. C. Cox. Speed estimation in wireless systems using wavelets. *IEEE Trans. Commun.*, 47(9):1357–1364, 1999.
- [10] M. V. Wickerhauser. *Adapted Wavelet Analysis from Theory to Software*. A. K. Peters, Wellesley, MA, 1994.